

# Frustrated Arrays of Nanomagnets for Efficient Reservoir Computing

Alexander J. Edwards\*, Dhritiman Bhattacharya<sup>†</sup>, Peng Zhou\*, Nathan R. McDonald<sup>‡</sup>, Lisa Loomis<sup>‡</sup>,  
Clare D. Thiem<sup>‡</sup>, Jayasimha Atulasimha<sup>†</sup>, Joseph S. Friedman\*

\*Department of Electrical and Computer Engineering, The University of Texas at Dallas, Richardson, TX  
{alexander.edwards, peng.zhou, joseph.friedman}@utdallas.edu

<sup>†</sup>Department of Mechanical and Nuclear Engineering, Virginia Commonwealth University, Richmond, VA  
bhattacharyad@mymail.vcu.edu, jatulasimha@vcu.edu

<sup>‡</sup>Air Force Research Laboratory - Information Directorate, Rome, NY  
{nathan.mcdonald.5, lisa.loomis.3, clare.thiem}@us.af.mil

**Abstract**—We simulated our nanomagnet reservoir computer (NMRC) design on benchmark tasks, demonstrating NMRC’s high memory content and expressibility. In support of the feasibility of this method, we fabricated a frustrated nanomagnet reservoir layer. Using this structure, we describe a low-power, low-area system with an area-energy-delay product  $10^7$  lower than conventional RC systems, that is therefore promising for size, weight, and power (SWaP) constrained applications.

**Keywords**—Reservoir Computing; Nanomagnet; Recurrent Neural Network; Neuromorphic Computing

## I. INTRODUCTION

A reservoir computer (RC) [1]–[4] is a powerful machine learning approach, employing a dynamic “reservoir” of recurrently connected computational nodes, which may be physically implemented by a wide range of devices with complex dynamics. Further, only the output layer of the network is trained via one line of linear algebra instead of typical iterative backpropagation techniques. Together, these advantages of RC greatly reduce the necessary overhead circuitry required for a full hardware realization.

A nanomagnet RC (NMRC) comprises a planar collection of nanomagnets. In [5], we demonstrated that the dynamics of the nanomagnets are sufficiently complex to serve as a reservoir layer. When several nanomagnets are placed in close proximity together, they induce frustration (Fig. 1).

In this work, we present initial experimental results demonstrating nanomagnet frustration and simulate NMRC solving tasks requiring high memory content. From these results, we propose that NMRC can be completely implemented in low-power, low area circuitry interfacing with CMOS, making it well-suited for SWaP-constrained or Internet of Things (IoT) platforms.

## II. NANOMAGNET RESERVOIR COMPUTING SYSTEM

The complete NMRC system of Fig. 2 contains three subsystems: reservoir inputs, readout, and output layer.

DISTRIBUTION STATEMENT A. Approved for public release; distribution is unlimited. AFRL-2021-0781

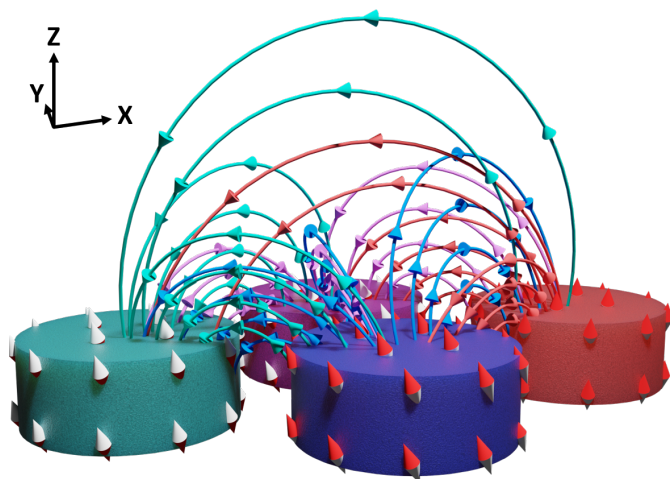


Fig. 1. Frustrated nanomagnets. Four nanomagnets with perpendicular magnetic anisotropy (PMA) are in close proximity to each other. Because adjacent nanomagnets with PMA are anti-ferromagnetically coupled, no single nanomagnet can be fully relaxed with its magnetization in the  $\pm z$  direction.

### A. Reservoir Inputs

Specific reservoir nanomagnets are designated as input nanomagnets. The state of the input nanomagnets can be written using spin-transfer torque (STT).

### B. Reservoir Readout

Each reservoir nanomagnet can be manufactured with a magnetic tunnel junction (MTJ) used for readout. Reading the resistance of the MTJ is equivalent to extracting the magnetization  $z$ -component of the free layer. A voltage divider is used to convert each MTJ resistance into a voltage level. The voltages are then fed into the linear output layer.

### C. Output Layer

Output weights are determined offline and written as conductances in a memristor crossbar array (MCA) [6]. The MCA performs the function of the output layer. This minimal circuitry enables a low-footprint interface to the reservoir.

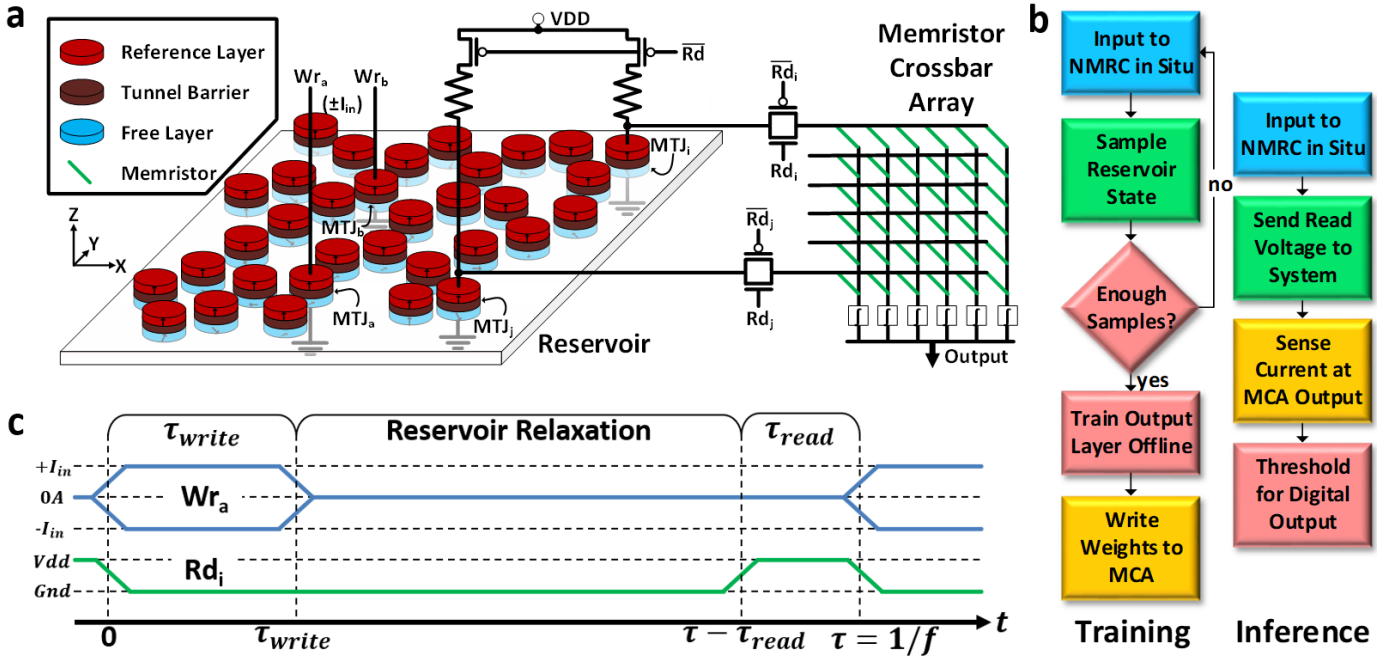


Fig. 2. Nanomagnet reservoir computing system diagram.

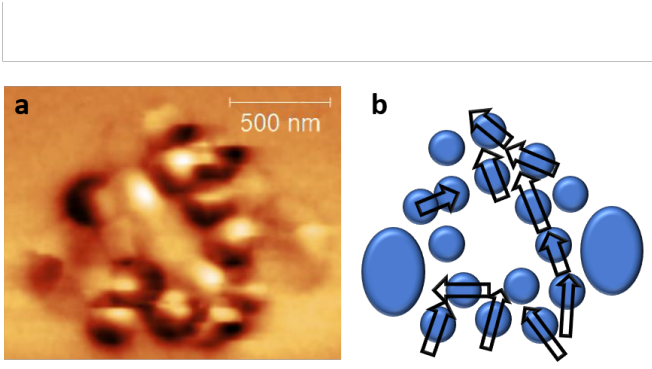


Fig. 3. (a) MFM image of fabricated reservoir. (b) Extracted magnetization directions. The magnetization of each nanomagnet points from the dark region to the light region.

### III. EXPERIMENTAL DEMONSTRATION

We manufactured a small nanomagnet reservoir via e-beam lithography which was performed using Raith 50 KV patterning tool on a Silicon substrate spin-coated with PMMA-495. After lithography, the substrate was developed in MIBK:IPA (1:3) solution for 30 seconds. A 13 nm layer of Cobalt was deposited at 0.3 Angstrom/s rate above a 7 nm Ti adhesion layer using an E-beam evaporator at base pressure of  $2e-7$  Torr. Finally lift-off was performed by soaking the sample in hot Acetone for 30 minutes.

Magnetic Force Microscopy was performed using Bruker AFM system using a High Moment tip. Nominal resonant frequency of the cantilever, lift height and scan rate were 70 kHz, 80 nm and 0.2 Hz respectively.

TABLE I  
SIMULATION PARAMETERS

Parameter	Description	Value	Unit
$M_{sat}$	Saturation Magnetization	$7.23e5$	$A/m$
$A_{ex}$	Exchange Stiffness	$1.3e-11$	$J/m$
$\alpha$	Gilbert Damping Factor	0.05	
$Ku_i$	Input Anisotropy	$3.62e5$	$J/m^3$
$Ku_r$	Reservoir Anisotropy	$1.05e5$	$J/m^3$
$D$	Nanomagnet Diameter	$30e-9$	$m$
$th$	Nanomagnet Thickness	$12e-9$	$m$
$\tau$	Input Period	$2.5 - 3e-8$	$s$
$T$	Temperature	0	$K$

An MFM image of the experiment is shown in Fig. 3(a), with magnetization directions visually extracted in Fig. 3(b). The nanomagnets were in a frustrated state as is evidenced by the fact that not all magnetizations lie on the same axis. This is an important step towards fabrication of a full NMRC system.

### IV. ADVANCED RESERVOIR TASKS

To further explore the capabilities of NMRC, we evaluated the performance of this paradigm on three tasks: triangle-square waveform identification, Boolean function evaluation, and an elementary cellular automata (ECA) observer.

Simulations were performed using Mumax3 [7], which approximates micromagnetic dynamics according to the Landau-Lifshitz torque equation. The simulation parameters used are presented in Table I.

#### A. Waveform Identification

In this task the nanomagnet reservoir must identify a triangle or square wave as depicted in figure 4. A single period of

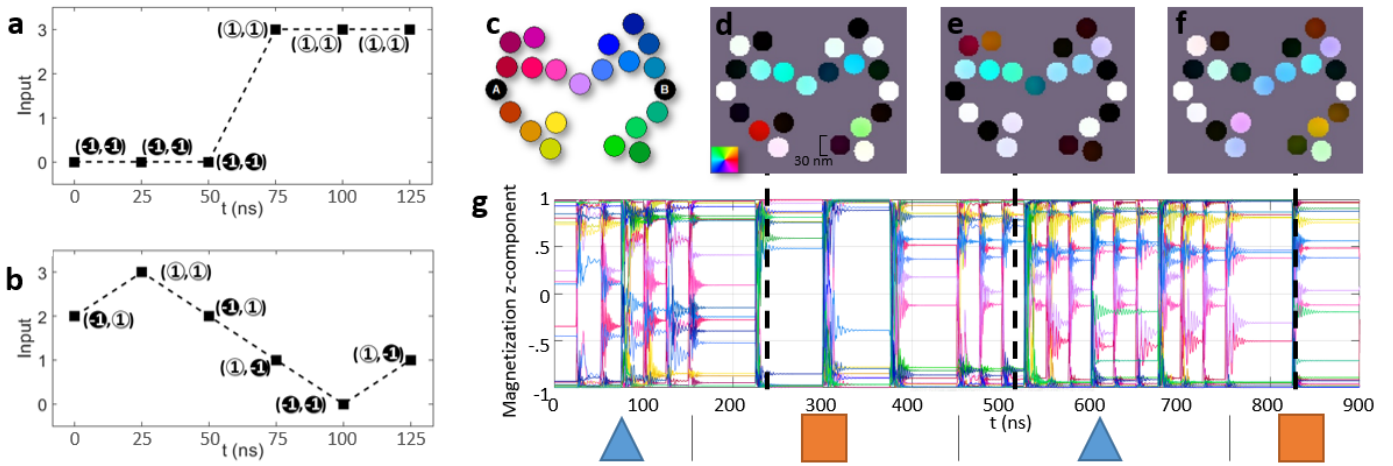


Fig. 4. (a-b) Square-wave and triangle-wave input sequences, respectively. (c) Reservoir layout. (d-f) Simulation snapshots. Colors represent the magnetization direction unit vector. White (black) represents magnetization along the  $+z$  ( $-z$ ) axis. Inset, color wheel indicating color directions. (g) Magnetization  $z$ -component transient. Colors of the traces match with nanomagnet colors in c.

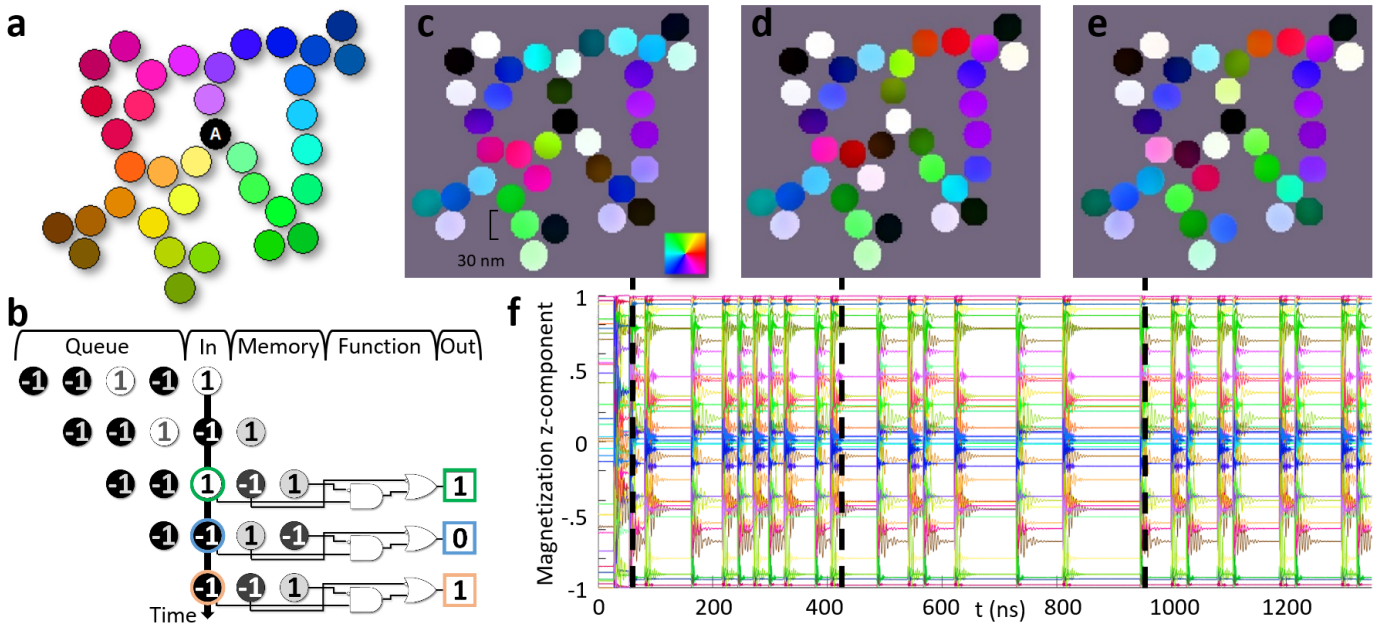


Fig. 5. (a) Nanomagnet reservoir layout. The nanomagnet marked with the letter A in the center of the reservoir is the input nanomagnet. All others are reservoir nanomagnets that are also used for readout. (b) Boolean function evaluation task depiction. Bits are fed into the input magnet over time. The reservoir must remember previous inputs and perform arbitrary Boolean functions on them. (c-e) Simulation snapshots of reservoir. (f) Magnetization  $z$ -component transient.

each type of wave was partitioned into six samples which were encoded with two-bit values and fed into the reservoir sequentially. Figure 4.a-b show the input sequences for the square and triangle waves respectively. Successive periods of triangle and square waves are fed into the reservoir randomly. The reservoir achieves 100% accuracy which is comparable to the results seen on a CMOS RC with 11 neurons indicating the reservoir's ability to perform temporal tasks.

### B. Boolean Function Evaluation

In this task the reservoir must compute all possible  $W$ -bit Boolean functions on a sequence of binary values provided

one bit at a time. (Fig. 5(b)). The simulated nanomagnet reservoir contained 35 nodes (Fig. 5(a)), and the magnetization directions varied in response to the input (Fig. 5(c-f)). The reservoir achieves 100% accuracy for  $W = 2$  and 3 bits and 92.4% for  $W = 4$  bits, which is comparable to the results seen on a CMOS RC with 25 neurons. These results indicate the reservoir's short-term memory capabilities, sufficient to perform complex calculations on data streams.

### C. ECA Observer

In the field of dynamical systems, an "observer" is trained to infer hidden state variables from a collection of known

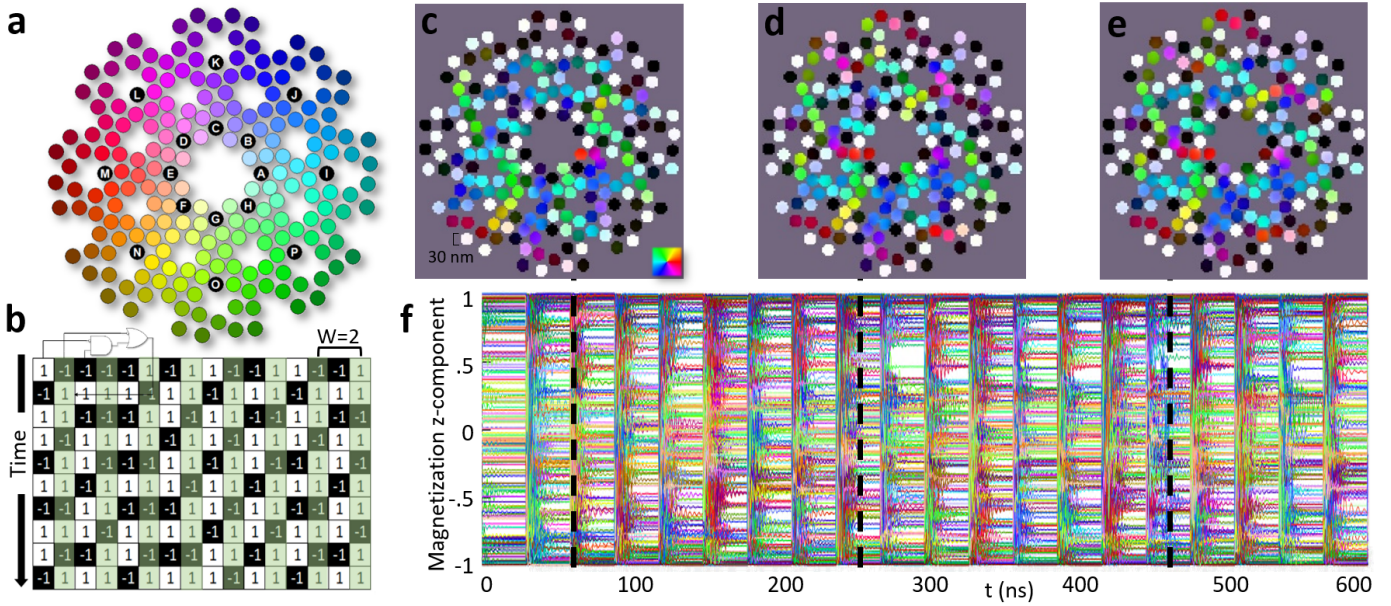


Fig. 6. (a) Reservoir layout for ECA observer task. Each input is duplicated for increased expressibility. Input pairs include nanomagnets A and I, B and J, C and K, etc. (b) ECA Observer task depiction. The RC must reproduce the entire ECA table having been presented only information from every  $W$ th column. (c-e) Simulation snapshots of reservoir. (f) Magnetization z-component transient.

TABLE II  
SUMMARY OF RESULTS FOR EACH TASK

RC Task	NMRC		Feed-Forward		CMOS RC	
	W	$\epsilon_{te}$	Memory	$\epsilon_{te}$	Neurons	$\epsilon_{te}$
Wave ID	N/A	0%	5 bits	21.0%	11	0%
Boolean Functions	2	0%	2 bits	0.4%	25	0%
	3	0%	3 bits	18.6%	25	0%
	4	7.6%	4 bits	15.3%	25	6.6%
ECA Observer	4	0.3%	6 bits	0%	35	0.2%
	8	6.7%	8 bits	6.5%	60	6.5%
	12	14.8%	7 bits	13.4%	45	14.8%
	16	17.5%	6 bits	17.4%	43	17.8%
	20	19.4%	8 bits	18.6%	56	19.4%
	24	22.8%	5 bits	22.4%	35	22.7%

state variables [8]. A 200 node reservoir (Fig. 6) was fed a subset of cell states from a vector array operated upon by the nonlinear elementary cellular automata (ECA) rule 59, and tasked to predict the state of all other cells in the array per time step. The reservoir achieved 99.7% accuracy, comparable to that of a CMOS RC with 35 neurons. This demonstrates the reservoir’s ability to integrate information from multiple concurrent inputs.

#### D. Results Summary

In order to establish a benchmark for the tasks, a simple single-layer perceptron network was created to perform the same tasks. Both present and past inputs were presented to this network. Table II presents the results for all three tasks comparing the performance of NMRC and the single-layer perceptron network, demonstrating the high memory content and expressivity of NMRC.

#### V. COMPUTATIONAL EFFICIENCY

We compared the area, energy, and minimum period of the NMRC to those of a CMOS RC which performed the same tasks with the same accuracy (see Table II). In the end, our system saw a reduction in area by 300,000x, in energy by 10x, and in period by 3x. The area-energy-delay product is therefore reduced by roughly seven orders of magnitude, making the system extremely well-suited to SWaP constrained environments.

#### VI. CONCLUSIONS

We demonstrate the applicability of NMRC in SWaP-constrained environments by presenting initial experimental results, showing the NMRC’s ability to perform complicated tasks, and describing low-power, low-footprint circuitry to integrate NMRC into a classical CMOS environment.

#### ACKNOWLEDGEMENT

Effort sponsored by the Air Force under contract number FA8750-15-3-6000. The U.S. Government is authorized to reproduce and distribute copies for Governmental purposes notwithstanding any copyright or other restrictive legends. The views and conclusions contained herein are those of the authors and should not be interpreted as necessarily representing the official policies or endorsements, either expressed or implied, of the Air Force or the U.S. Government. The authors thank E. Laws, J. McConnell, N. Nazir, L. Philoon, and C. Simmons for technical support, and the Texas Advanced Computing Center at The University of Texas at Austin for providing computational resources. VCU authors acknowledge NSF grants CCF 1815033 and ECCS 1954589. Fabrication and characterization was carried out at VCU VMEC and NCC.

## REFERENCES

- [1] H. Jaeger, "The "echo state" approach to analysing and training recurrent neural networks-with an erratum note'," *Germ. Nat. Res. Cent. for Info. Tech.*, vol. 148, 2001.
- [2] W. Maass *et al.*, "Real-time computing without stable states: a new framework for neural computation based on perturbations." *Neural Comput.*, vol. 14, no. 11, 2002.
- [3] H. Jaeger *et al.*, "Harnessing nonlinearity: Predicting chaotic systems and saving energy in wireless communication," *Science*, vol. 304, no. 78, 2004.
- [4] G. Tanaka *et al.*, "Recent advances in physical reservoir computing: A review," *Neural Networks*, vol. 115, 2019.
- [5] P. Zhou *et al.*, "Reservoir computing with planar nanomagnet arrays," *GOMAC*, 2020.
- [6] F. Cai *et al.*, "A fully integrated reprogrammable memristor-CMOS system for efficient multiply-accumulate operations," *Nature Electronics*, vol. 2, no. 7, 2019.
- [7] A. Vansteenkiste *et al.*, "The design and verification of Mumax3," *AIP Adv.*, vol. 4, no. 10, p. 107133, 2014.
- [8] Z. Lu *et al.*, "Reservoir observers: Model-free inference of unmeasured variables in chaotic systems," *Chaos*, vol. 27, no. 4, 2017.